On the choice of the number of samples in laser Doppler anemometry signal processing

Federico Dios, MEMBER SPIE
Adolfo Comerón, MEMBER SPIE
David García-Vizcaíno
Universitat Politècnica de Catalunya
Department of Signal Theory
and Communication
C/Gran Capità s/n. Campus Nord, D-3
08034 Barcelona, Spain
E-mail: fede@tsc.upc.es

Abstract. The minimum number of samples that must be taken from a sinusoidal signal affected by white Gaussian noise, in order to find its frequency with a predetermined maximum error, is derived. This analysis is of interest in evaluating the performance of velocity-measurement systems based on the Doppler effect. Specifically, in laser Doppler anemometry (LDA) it is usual to receive bursts with a poor signal-to-noise ratio, yet high accuracy is required for the measurement. In recent years special attention has been paid to the problem of monitoring the temporal evolution of turbulent flows. In this kind of situation averaging or filtering the data sequences cannot be allowed: in a rapidly changing environment each one of the measurements should rather be performed within a maximum permissible error and the bursts strongly affected by noise removed. The method for velocity extraction that will be considered here is the spectral analysis through the squared discrete Fourier transform, or periodogram, of the received bursts. This paper has two parts. In the first an approximate expression for the error committed in LDA is derived and discussed. In the second a mathematical formalism for the exact calculation of the error as a function of the signal-to-noise ratio is obtained, and some universal curves for the expected error are provided. The results presented here appear to represent a fundamental limitation on the accuracy of LDA measurements, yet, to our knowledge, they have not been reported in the literature so far. [DOI: 10.1117/1.1361107]

Subject terms: Doppler effect; laser anemometry; metrology; noise.

Paper 200135 received Apr. 3, 2000; revised manuscript received Dec. 14, 2000; accepted for publication Dec. 14, 2000.

1 Introduction

Laser Doppler anemometry (LDA) systems for measuring flow velocities, widely used in industry and research,[1–5] present intrinsic advantage over classical methods. These attractive features are the noninvasive nature of the measurement, its high spatial resolution (some hundreds of micrometers over 2 or 3 mm typically), and its precision (about 1%). In recent years research on the improvement of LDA systems has been directed, among other aspects, towards its application to turbulent flows.[6–10] The spatial resolution takes on major importance in this context, because high velocity gradients, widening the spectrum of the received signals, may take place in the flow. Moreover, this application emphasizes the trade-off between two important features of the system, namely, the precision and the measurement rate. Capturing systematically a large number of samples to minimize the frequency error requires a large amount of memory, and the processing will be slow. It is also possible to separate the acquisition and the processing of the captured samples, although this alternative is not always desirable.

In order to maintain the error below a fixed, predetermined limit independently of the kind of situation under investigation, it is important to have some reasonable idea about the required number of samples. The frequency error will be dependent on the number of samples, the signal-to-noise ratio, and the sampling frequency. Moreover, due to the discrete, digital nature of the processing, the relative position of the true spectrum maximum with respect to the position of the samples in the DFT will have also some influence. All these aspects of the problem are treated in what follows.

2 Frequency Error and Spectral Width

2.1 *The Number of Fringes*

The relationship between the Doppler frequency shift f_D of the signal received from a moving particle and its velocity v is, in the differential LDA scheme,[11,12]

$$f_D = \frac{v}{s_f} = \frac{2v \sin(\alpha/2)}{\lambda}, \tag{1}$$

s_f being the separation between the interference fringes formed at the crossing point of the laser beams (the so-called scattering volume), α the angle between the directions of the beams, and λ the wavelength in the fluid under measurement. From (1) we obtain

$$\frac{\Delta v}{v} = \frac{\Delta f_D}{f_D}. \tag{2}$$

 0091-3286/2001/$15.00

This equation is usually interpreted as the relationship between the relative error committed in the velocity measurement and the relative signal spectral width. Necessarily the optical signal has a finite duration, τ, which is proportional to the waistsize of the beams at the crossing point and inversely proportional to the particle velocity. Assuming a transverse Gaussian variation of the beams, the spectral width can be written as

$$\Delta f_D = \frac{2}{\pi \tau}. \tag{3}$$

This expression is exact when the temporal duration τ is measured between the points (crossed by the particle) at which the beam field has decayed to $1/e$ times the maximum, and the spectral width is defined as the separation between the points on the frequency axis at which the spectrum amplitude has fallen to $e^{-1/4}$ with respect to the peak. Although other possible criteria for defining the signal duration and the spectral width would be valid, we will use that convention.

The fringes formed in the scattering volume are steady for beams having the same frequency. Combining the previous expressions, the time interval τ can be expressed as a function of the particle velocity and the spatial dimensions. The relative error in the velocity measurement can be written as

$$\frac{\Delta v}{v} = \frac{2}{\pi n_f}, \tag{4}$$

n_f being the number of interference fringes.

Equation (4) clearly shows that the frequency error may be reduced by increasing the parameter n_f through the probe design.

Practical systems are however more complex, because of the need for measuring the sign of the velocity. In most real LDA systems an acusto-optic modulator (AOM), acting as a frequency shifter, is placed in the path of one of the laser beams. The interference fringes are not steady any longer; instead they move along the transverse direction with a velocity

$$v_f = f_{AOM} s_f, \tag{5}$$

f_{AOM} being the frequency shift. Now the effective number of fringes crossed by a particle traveling across the scattering volume is

$$n'_{eff} = \tau(f_{AOM} \mp |f_D|). \tag{6}$$

An appropriate design of the system forces the fringes' phase velocity to be higher than the maximum velocity to be expected in the flow, so that $f_{AOM} > f_D$ in all cases; otherwise the sign ambiguity will not be completely resolved. The sign in Eq. (6) is negative if the particle moves in the same direction as the fringes, and positive if it moves oppositely.

Received signals must be converted to a digital format to be processed by a computer. Maintaining high frequencies at this point is not practical, due to the price of high-velocity analog-to-digital (AD) conversion cards with sufficient resolution. So it is highly recommended to convert the received signals to an intermediate frequency, f_I, by mixing the burst with a local oscillator of appropriate frequency. The effective number of periods is then

$$n_{eff} = \tau(f_I \mp |f_D|) \tag{7}$$

with

$$f_I = |f_{AOM} - f_{LO}|, \tag{8}$$

f_{LO} being the local-oscillator frequency. Finally, the relative error can be written:

$$\frac{\Delta f}{f} = \frac{\Delta f_D}{f_I \mp |f_D|} = \frac{2}{\pi n_{eff}}. \tag{9}$$

2.2 *The Acquisition Process*

The signal centered at the intermediate frequency is filtered to separate the continuous component—the so-called *pedestal*—from the high-frequency components of the burst, because the useful information is only in the modulating signal. This step is important to reduce the dynamic range necessary in the AD conversion unit. The pedestal of the signal may be used to trigger the conversion process.

Following the Nyquist criterion, the sampling frequency used in the acquisition must be

$$f_{SAMP} > 2(f_I + |f_D|_{MAX}). \tag{10}$$

At this point the question arises of the number of samples to be captured in a burst to assure a minimum error in the extraction of the velocity.

It may happen that it is not practical to acquire the whole burst generated from each particle, due to the system memory limitation and because the process would be highly time-consuming. Moreover the burst duration itself is *a priori* unknown, as it is a direct function of the particle velocity. Then there is an available number of periods in the bursts, n_{eff}, but a lesser number of periods, n, that will actually be captured. If we desire to capture samples only within the burst (outside it there is only noise), then the condition must be

$$n_{eff} \geqslant n = N \frac{f_I \mp |f_D|}{f_{SAMP}}, \tag{11}$$

N being the number of samples. Finally, the expected error may be written as follows:

$$\frac{\Delta v}{v} = \frac{2}{\pi n} = \frac{2}{\pi} \frac{f_{SAMP}}{f_I \mp |f_D|} \frac{1}{N} \tag{12}$$

with the constraint given by

$$N \leqslant N_{MAX} = \tau f_{SAMP}, \tag{13}$$

which is dependent on the particle velocity. Usually one takes the maximum possible number of samples in the worst case, i.e., with the maximum velocity.

From Eq. (12) it is apparent that the relative error is dependent on the velocity being measured at each moment. In a LDA apparatus it is not easy to adjust the parameters in real time during the measurements. This is due to the discontinuous nature of the signal and because rapid changes in the fluid can take place at any time. So the number of captured samples, N, and the sampling frequency may be only roughly adjusted for each situation.

The error margin is given by

$$\left.\frac{\Delta v}{v}\right|_{\mathrm{MIN}} = \frac{2}{\pi}\frac{f_{\mathrm{SMP}}}{f_{\mathrm{I}}+|f_{\mathrm{D}}|_{\mathrm{MAX}}}\frac{1}{N},$$
$$\left.\frac{\Delta v}{v}\right|_{\mathrm{MAX}} = \frac{2}{\pi}\frac{f_{\mathrm{SMP}}}{f_{\mathrm{I}}-|f_{\mathrm{D}}|_{\mathrm{MAX}}}\frac{1}{N} \tag{14}$$

3 Noise and Signal-Processing Considerations

In the LDA photoreceiver we will find all the types of noise that may currently appear in an optoelectronic system, i.e., thermal noise, shot noise from the photodetection process and from the electronic devices, and quantization noise after the AD conversion. However, in the previous analysis the influence of the noise on the signal was not considered in an explicit form. Actually this point was not necessary for our purposes. Because we were assuming that the error in the determination of the Doppler frequency was proportional to the signal spectral width, we were accepting that some kind of noise is added to the burst, which leads to an error in the determination of the spectral maximum: if our spectrum were a sharp, delta-type one, then it would be possible to find its maximum even with a very low signal-to-noise ratio, and, conversely, if there were no noise at all, then the spectral width and the number of captured samples would be irrelevant, because we always could locate the maximum with a precision limited only by the frequency interval in the discrete estimated spectrum.

Some modern commercial LDA systems perform the autocorrelation of the received signal in order to reduce the noise. With the resulting sequence of data the accuracy in the extraction of the Doppler frequency is improved. However, this noise reduction is proportional to the number of samples taken for the autocorrelation, so the basic question about the necessary minimum number of samples still occurs.[13,14]

Another important point to be considered is that in the processing stage we are working with a digital sequence. If a direct spectral analysis is being done by means of a discrete Fourier transform, then we have to decide where the maximum of the true spectrum is exactly, which will seldom coincide with the position of one of the samples. Letting f_{SAMP} be the sampling frequency and N the number of samples, and assuming a noiseless situation, we have a maximum possible error in the determination of the exact frequency as large as

$$\delta f = \frac{1}{2}\frac{f_{\mathrm{SAMP}}}{N}. \tag{15}$$

The noise has another practical effect, namely the reduction of the effective burst duration. The ends of the burst, at which the pedestal has a very low amplitude, are so affected by noise that they do not contain useful information. Due to the large range of possible burst amplitudes, depending on the particle size, it is not possible to apply a constant coefficient of temporal reduction of the signal. A minimum acceptable signal-to-noise ratio could be included as a validation threshold.

4 Exact Calculation of the Frequency Error

4.1 *Noise-Free Sequences*

In the absence of noise, the error comes from the fact that we are sampling the signal with a finite number of samples. It can be easily shown that the mean error in determining the peak of the spectrum of a sinusoidal, noise-free, digitized sequence is

$$\varepsilon_f = \frac{\Delta f}{4}, \tag{16}$$

Δf being now the separation between frequency samples. The variance of this error is

$$\sigma^2_{\varepsilon f} = \frac{(\Delta f)^2}{48}. \tag{17}$$

These values have been calculated under the assumption that the frequency to be estimated can take any value within the interval Δf with equal probability. However, in the absence of noise and by means of successive application of zero padding or other interpolation techniques,[15] the value of Δf and, consequently, the error may be made arbitrarily small (at the cost of increasing the calculation time).

4.2 *Noisy Signals*

In the presence of noise the situation is clearly different. Usually the signal-to-noise ratio available in a LDA system is low, and it is necessary to know how the accuracy of the measurements is being affected by noise. The objective of this section is to calculate the frequency error in the determination of the spectral peak as a function of the signal-to-noise ratio and of the number of samples used in the analysis. We will suppose that white, Gaussian-type noise is added to our sinusoidal sequence. Section 7 contains a list of symbols used in this analysis.

The frequency error is defined as

$$\varepsilon_f = |f'_{\max} - f_{\max}|, \tag{18}$$

$f_{\max}$ being the position of the peak in the true spectrum of the noise-free signal, and $f'_{\max}$ the position of the sample in which the noisy discrete spectrum has its maximum. The peak frequency of the true spectrum, $f_{\max}$, is a real and arbitrary value within the possible range of frequencies; $f'_{\max}$, however, can only take discrete values in this range. We can write

$$\varepsilon_f = |k'_{\max} - x_{\max}|\,\Delta f \tag{19}$$

with $k'_{\max}$ an integer and $x_{\max} = f_{\max}/\Delta f$ a real number.

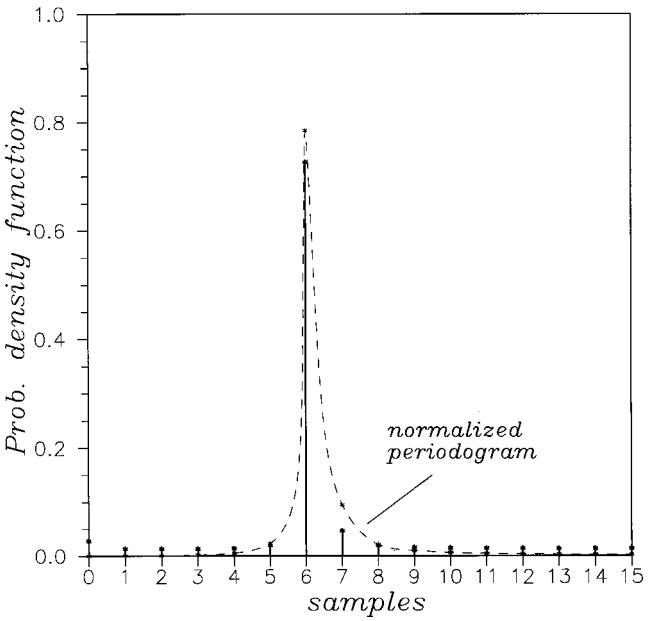

Fig. 1 The comb-type probability density function of the position of the periodogram peak for a noisy sinusoidal signal. A scaled version of the noise-free periodogram is shown (dashed line). Only one half of the symmetrical spectrum is shown.

Due to the noise, *all the samples in the spectrum have some probability of becoming the position of the measured peak*. We can build a discrete probability density function showing this fact, in the form

$$f_x(x)=\sum_{k=0}^{N/2-1} p_k\delta(x-k), \tag{20}$$

p_k being the probability assigned to each sample to be taken as the maximum of the noisy spectrum, and $\delta(x)$ the Dirac delta.

In order to find both the mean error committed in the determination of the frequency and its variance, the coefficients p_k will have to be calculated. In Sec. 4.4 these probabilities will be derived. In Fig. 1 the probability density function written in Eq. (20) for an arbitrary case is shown.

From Eqs. (19) and (20) we obtain the mean and the variance of the frequency error as

$$\langle \varepsilon_f\rangle=\overline{\varepsilon_f}=\sum_{i=0}^{N/2-1} p_i|x_{\max}-i|\,\Delta f \tag{21}$$

and

$$\langle(\varepsilon-\overline{\varepsilon})^2\rangle=\sum_{i=0}^{N/2-1} p_i|x_{\max}-i|^2(\Delta f)^2 - \left(\sum_{i=0}^{N/2-1} p_i|x_{\max}-i|\,\Delta f\right)^2. \tag{22}$$

4.3 *Noise Statistics*

The complete analysis is not straightforward, due to the change in the noise statistics during the DFT procedure and, especially, to the fact that one usually works with the periodogram (the squared modulus of the DFT). Thus, we can assume that each temporal sample of the burst has an added Gaussian-type noise, but this is not true in the periodogram. The situation is described below.

We have a noisy temporal sequence of the form

$$s[n]=x[n]+g[n], \tag{23}$$

$x[n]$ being the sequence corresponding to a sinusoidal signal and $g[n]$ the Gaussian-type noise sequence. This is a simple model, but accurate enough for our purposes. The DFT yields

$$S[k]=X[k]+G[k], \tag{24}$$

and the squared modulus of the DFT is

$$|S[k]|^2=|X[k]|^2+G[k]X^*[k]+G^*[k]X[k]+|G[k]|^2. \tag{25}$$

We can observe that the noise affecting the squared modulus of $X[k]$ is composed of two different terms. The first one is

$$N_1[k]=|G[k]|^2=G[k]_{\mathrm{re}}^2+G[k]_{\mathrm{im}}^2, \tag{26}$$

whose statistics follows a chi-square density function with two degrees of freedom, because it has been obtained as the sum of two independent squared Gaussian random variables.[16] The chi-square function with two degrees of freedom is actually the exponential density function: $f_{N_1}(N_1)=\lambda\exp(-\lambda N_1)$. The mean and the standard deviation of such a random variable are identical, and in our case it can be easily proved that their value is N, the number of samples, for any value of k.

The other noise term is

$$N_2[k]=G[k]X^*[k]+G^*[k]X[k]=2(X_{\mathrm{re}}G_{\mathrm{im}}+X_{\mathrm{im}}G_{\mathrm{re}}). \tag{27}$$

We can consider that the samples of the DFT sequence $X[k]$ are known and consequently can be treated as constants. This point of view simplifies the statistical problem; however, we will be forced to state precisely the value of frequency for which the error is calculated. In Sec. 5 we will see the practical consequences of this choice. This second term of the noise is a Gaussian random variable superimposed on each sample in the periodogram. Assuming that $g[n]$ (and thus $G[k]$) has zero mean, the same is true for $N_2[k]$. The calculation of the variance is somewhat complicated, and we will omit the details. It can in fact be proved, however, that

$$\sigma_{N_2}^2=\begin{cases} 2N|X[k]|^2\sigma_g^2 & \text{for } k\neq 0,\\ 4N|X[0]|^2\sigma_g^2 & \text{for } k=0,\end{cases} \tag{28}$$

N being the number of samples and σ_g^2 the variance of the temporal noise samples $g[n]$.

The noise in the periodogram is the sum of the two terms, as we have just seen. The next step is finding the

probability distribution, in order to estimate its influence in the determination of the spectrum peak. Unfortunately, the two terms of noise, $N_1[k]$ and $N_2[k]$, are not independent random variables.

We write the total noise as

$$z = N_1[k] + N_2[k], \tag{29}$$

and after rather laborious calculation following a standard procedure,[17] its density function can be obtained as

$$f_z(z) = \frac{\exp(-z/2\sigma^2)}{2\pi\sigma^2} \exp\left(-\frac{|X|^2}{\sigma^2}\right) \times \int_{-\pi/2}^{\pi/2} \exp\left[-\frac{\sin t}{\sigma^2}|X|(|X|^2+z)^{1/2}\right] dt. \tag{30}$$

for $z > -|X|^2$ and with $\sigma^2 = (N/2)\sigma_g^2$.

For the sample located at the origin in the periodogram, $k=0$, the situation is different. It occurs that $X_{\mathrm{im}}[0] = G_{\mathrm{im}}[0] = 0$ and then we have

$$z = N_1[0] + N_2[0] = G_{\mathrm{re}}^2[0] + 2X_{\mathrm{re}}[0]G_{\mathrm{re}}[0], \tag{31}$$

with somewhat different statistics because we are now adding a chi-square random variable of order one to a Gaussian one. Again after laborious calculations, the density function results:

$$f_z(z)|_{k=0} = \frac{1}{\sigma\sqrt{2\pi}} \frac{\exp\{(-z+2|X[0]|^2)/2\sigma^2\}}{\sqrt{z+|X[0]|^2}} \times \cosh\left\{\frac{|X[0]|}{\sigma^2}(z+|X|[0]|^2)^{1/2}\right\} \tag{32}$$

for $z > -|X[0]|^2$ and with $\sigma^2 = N\sigma_g^2$.

4.4 *Calculation of the Probabilities p_k*

As noted above, N is the total number of samples, although we only analyze one half of the periodogram, due to its symmetry. As we will apply the zero-padding technique (once, twice, or more times) we have to take into account that the number N' of captured samples is different from the number N used in the calculations. The relationship between them is $N = N' \times 2^{n_{\mathrm{zp}}}$, n_{zp} being the number of times the zero-padding technique is applied.

The probability p_k for sample k to become the peak of the spectrum due to the noise is difficult to calculate in a direct approach, because the number of samples is usually large, but it can be obtained by means of an indirect method, as explained below.

At the first step we determine the range of values on the periodogram amplitude axis that any of the random variables (the samples) may take. Theoretically this range extends from zero to infinity, but in practice we can establish a reasonable limit as a function of the SNR value, with negligible error. If this range of amplitudes $(0, A_{\max})$ is partitioned into L small intervals, we can write

$$p_k = P\{S_k \to \max\} = \sum_{l=0}^{l=L-1} P\{S_k \to \max,\ S_k \in (A_1, A_{l+1})\}, \tag{33}$$

where $A_0 = 0$ and $A_L = A_{\max}$. The expression $S_k \to \max$ means the event ''the value $|S[k]|^2$ has become the peak of the periodogram.'' The expression $P\{\xi_1, \xi_2\}$ means the probability of two events ξ_1 and ξ_2 occurring simultaneously.

Each one of the terms in the sum on the right-hand side of Eq. (33) may be transformed as follows:

$$P\{S_k \to \max,\ S_k \in (A_l, A_{l+1})\} = P\{S_0, S_1, \ldots, S_{k-1}, S_{k+1}, \ldots, S_{N/2-1} < A_l, A_l < S_k < A_{l+1}\}. \tag{34}$$

Actually, as can be easily noticed, this last equation is only an approximation, unless the number L of intervals in the partition tends to infinity. However, we will take a value for L large enough as to commit a negligible error. The calculations must be performed numerically.

The probability appearing in the right-hand member of Eq. (34) may be rewritten as

$$P\{S_k \to \max,\ S_k \in (A_l, A_{l+1})\} = P\{A_l < S_k < A_{l+1}\} \prod_{\substack{j=1 \\ j \neq k}}^{N/2-1} F_{S_j}(A_l), \tag{35}$$

$F_{S_j}(A_l)$ being the value of the probability distribution function of the random variable S_j in A_l. We have now

$$P\{S_k \to \max\} = \sum_{l=0}^{L-1} P\{S_k \to \max,\ S_k \in (A_l, A_{l+1})\} = \sum_{l=0}^{L-1} P\{S_k \in (A_l, A_{l+1})\} \prod_{\substack{j=0 \\ j \neq k}}^{N/2-1} F_{S_j}(A_l). \tag{36}$$

Finally we use the equality $P\{S_k \in (A_l, A_{l+1})\} = F_{S_k}(A_{l-1}) - F_{S_k}(A_l)$ to write the probability for each sample to be the peak of the spectrum:

$$p_k = P\{S_k \to \max\} = \sum_{l=0}^{L-1} \left[\left(\frac{F_{S_k}(A_{l+1})}{F_{S_k}(A_l)} - 1\right) \prod_{j=0}^{N/2-1} F_{S_j}(A_l)\right]. \tag{37}$$

Substituting Eq. (37) in Eqs. (21) and (22), the mean of the frequency error and its variance may be calculated.

5 Numerical Results

By means of the numerical computation of the preceding formalism it can be seen that the error is primarily conditioned by the relative position of the real spectral peak (the signal frequency) in the discrete scale of frequencies: as was mentioned above, the error is minimized if the peak falls at the position of one of the samples and, contrariwise, it is maximum when the real peak falls in the middle of the

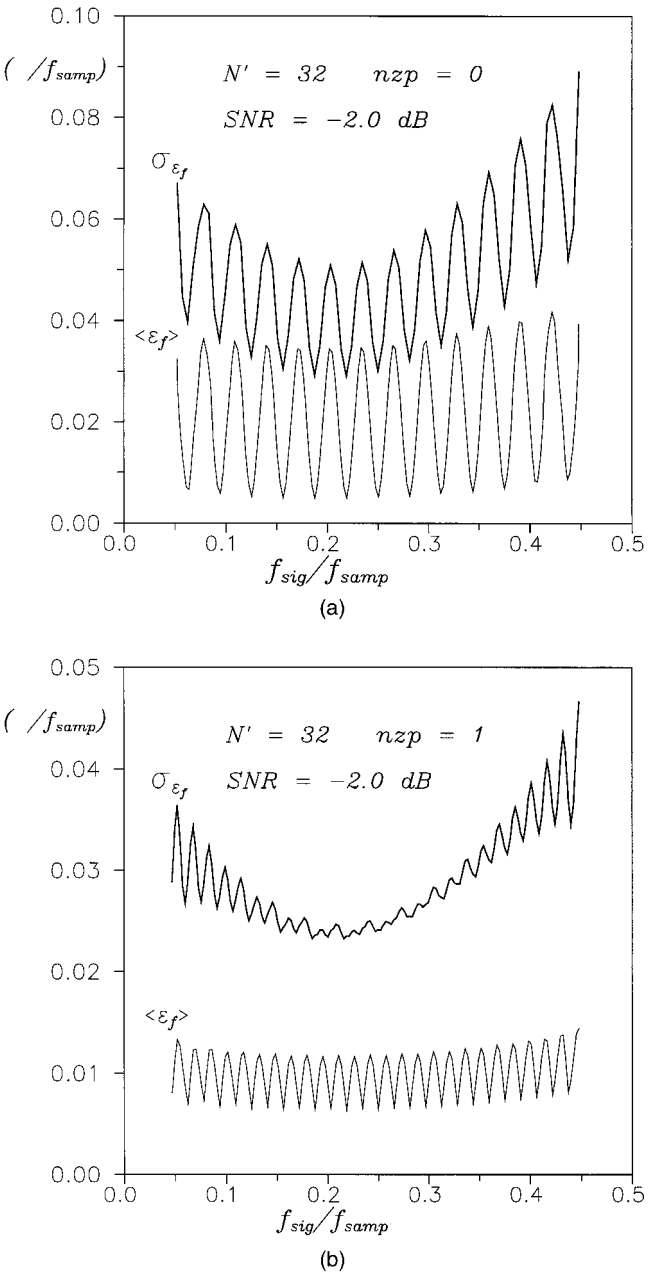

Fig. 2 Mean and standard deviation of the frequency error as functions of the frequency signal with 32 samples extracted from the signal. Both axes have been normalized to the sampling frequency. The number of times the zero-padding technique was applied is 0 in (a) and 1 in (b).

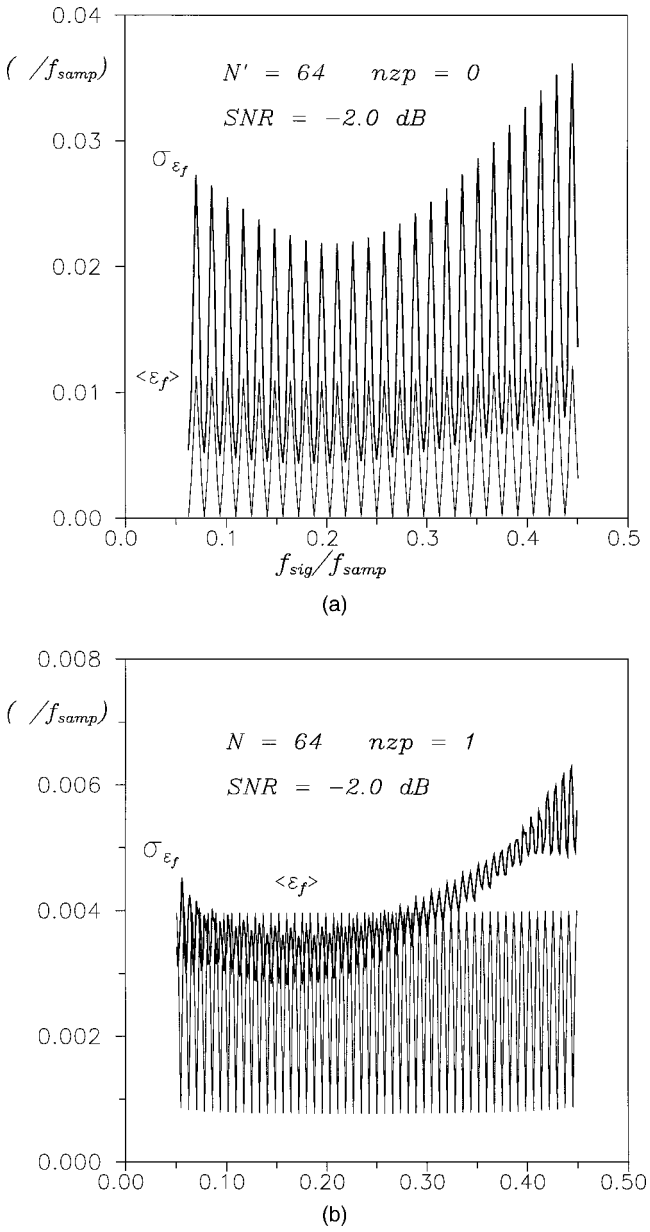

Fig. 3 Same as in Fig. 2, but with $N' = 64$.

frequency interval. This fact is apparent in Fig. 2 and 3. In these curves the mean and the standard deviation of the error (normalized to the sampling frequency) have been plotted as functions of the signal frequency (again normalized to the sampling frequency) and for SNR $= -2.0$ dB. The numbers of captured samples are 32 and 64, respectively, and the number of times that the zero-padding interpolation was applied (n_{zp}) is different for each one of the two graphs shown in the figures. It can be observed from these curves that on applying the zero-padding technique the ripple in the error curves diminishes. Moreover, in agreement with the technique of maximum-likelihood estimation, the error is larger when the signal frequency is close to zero or to the Nyquist limit.[18]

The curves of Fig. 4 show the mean error and the standard deviation as a function of the SNR for two different values of frequency. One of the signal frequencies was chosen falling just on the position of a sample (minimum error), and the other one falling in the middle of the frequency interval (maximum error). The numbers of real samples were $N' = 16$, 32, 64, and 128, respectively. There are several curves in each figure: solid lines correspond to the frequency-error standard deviation, and dashed lines to the mean frequency error. Fine lines are for the maximum-error case, and coarse lines for the minimum. The interpretation of these plots is straightforward. In any of them a SNR limit or threshold can be seen, above which the error diminishes very rapidly. Plots have been made from the

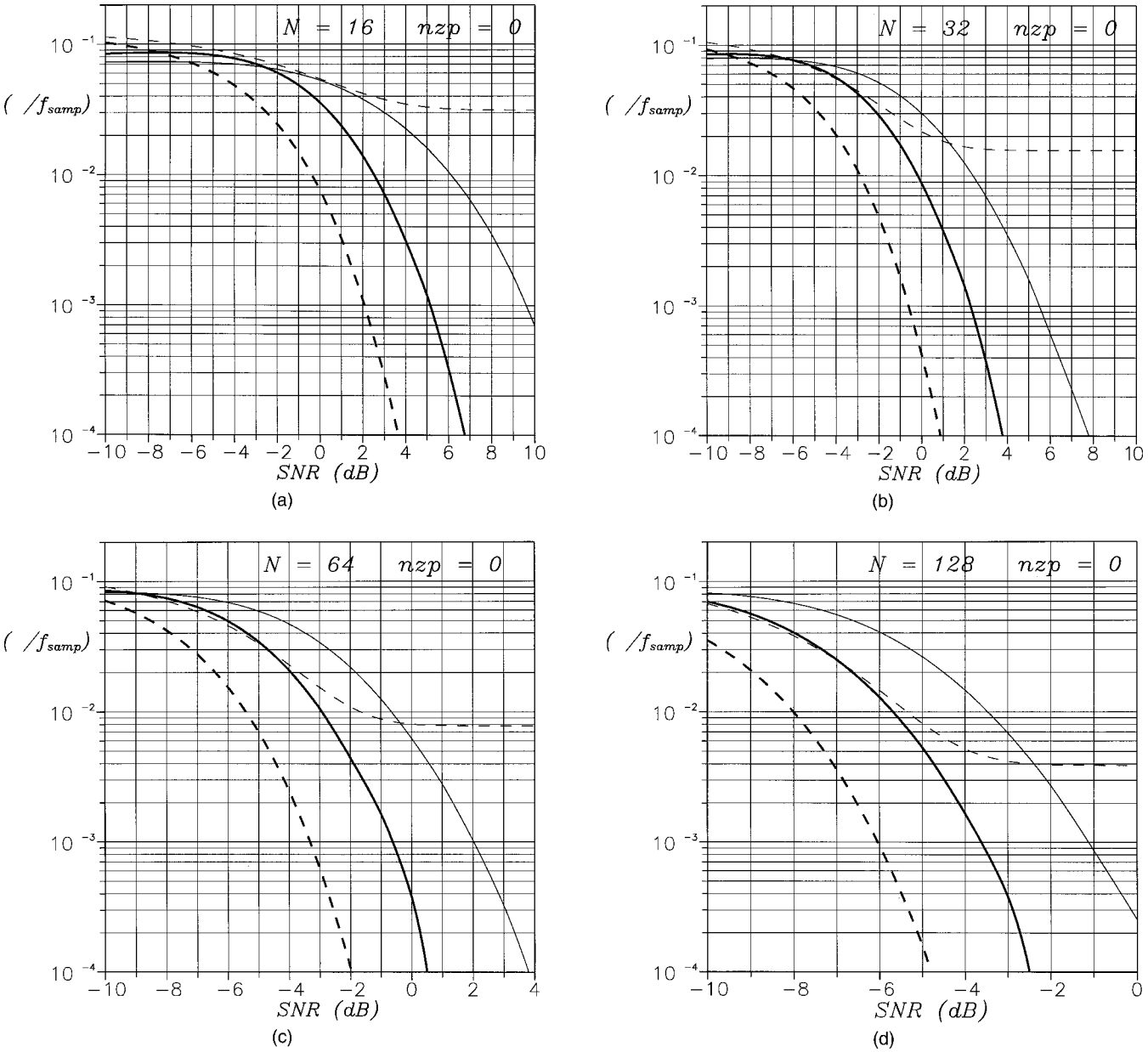

Fig. 4 Mean (dotted line) and standard deviation (solid line) of the frequency error, normalized to the sampling frequency, as a function of the signal-to-noise ratio, for some fixed values of signal frequency. Fine lines correspond to the worst case, with a frequency value lying in the middle of the interval between two samples. Coarse lines are for the best case, with a frequency value just on a sample location. Different plots correspond to different numbers of captured samples.

lower value of −10 dB, following the work of Qui et al.,[19] who demonstrated the possibility of detecting bursts with a low SNR.

Finally, the plots in Fig. 5 are similar to the preceding ones, but now all curves have been calculated with the same total number of samples [$N=64$ in Fig. 5(a), and $N=128$ in Fig. 5(b)] and only for the case of the signal frequency lying at the position of a sample (minimum error). The difference from the curves in Fig. 4 lies in the number of real samples and in the times at which the interpolation technique was applied. From these curves it can be concluded that, although the zero-padding technique improves the frequency estimation, having as many temporal samples as possible within the technological constraints, even with very poor SNR, is better than applying that interpolation technique to reach the same number of samples.

6 Conclusions

An especially important point for an accurate application of signal-processing techniques in LDA, not always enough remarked, is maintaining the number of samples taken in each burst above a minimum value. A numerical procedure to calculate the error in the estimation of the Doppler frequency taking into account the expected signal-to-noise ratio has been developed. The mathematical procedure reported above permits one to assess in practice how many

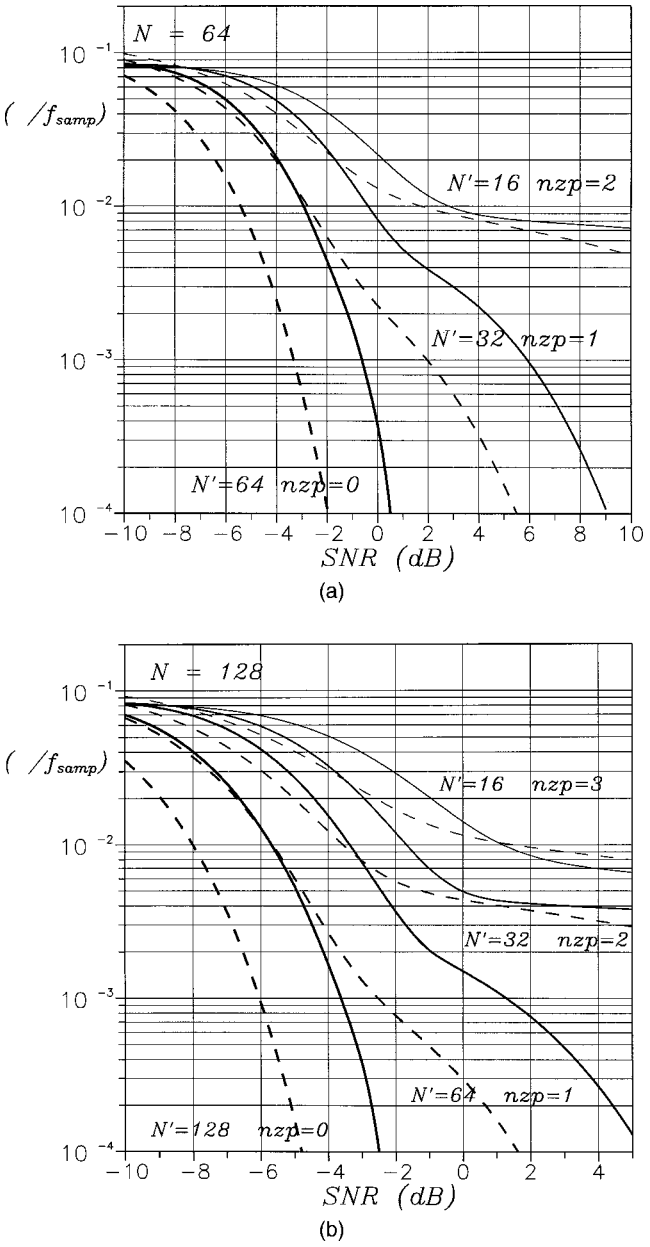

Fig. 5 Mean (dotted lines) and standard deviation (solid lines) of the frequency error as a function of the signal-to-noise ratio. All curves were calculated for the best case, with the signal frequency lying at a sample location. The exact value $f_{sig}/f_{samp}=0.21875$ is taken. In (a) the number of samples used in the analysis is $N=64$, and in (b) it is $N=128$. The difference between the curves is due to the number of real samples taken (N') and the number of zero-padding interpolations applied (r_{zp}).

samples in the burst have to be captured to perform the signal processing with a guaranteed maximum error in the frequency estimation. We think the obtained curves are in fact universal and can be used for most situations.

7 Appendix

Some of the symbols used in the mathematical developments in Sec. 4 are listed below.

f	received rf signal frequency
$f_{\max}, f'_{\max}$	position of the true spectrum peak and position of the discrete noisy spectrum peak
$f_x(x)$	probability density function
f_{AOM}	acusto-optic frequency shift
f_{D}	Doppler shift
f_{I}	intermediate frequency
f_{LO}	local-oscillator frequency
f_{SAMP}	sampling frequency
$g[n], G[k]$	additive-Gaussian-noise temporal sequence and its discrete spectrum
n_{zp}	number of times the zero padding technique is applied to the captured samples
p_k	probability for the kth sample in the periodogram to be taken as the maximum, due to the addition of noise
$s[n], S[k]$	received noisy temporal sequence and its discrete spectrum
$x[n], X[k]$	pure noiseless sinusoidal sequence and its discrete spectrum
z	total noise in the periodogram
$\varepsilon_f, \langle \varepsilon_f \rangle$	frequency error and mean frequency error
σ_g^2	temporal Gaussian noise variance
$\sigma_{\varepsilon_f}^2$	frequency error variance
A_l, A_{l+1}	periodogram amplitude limits for the $l+1$ interval
$A_0, A_{\max}$	minimum and estimated maximum amplitude values in the signal periodogram
$F_{Si}(A_j)$	probability distribution function of the periodogram ith sample at the value A_j (i.e., $P\{S[i] \leqslant A_j\}$)
N, N'	number of samples used in the calculation of the spectrum and number of captured signal samples
$N_1[k], N_2[k]$	the two components of noise present in the received signal periodogram
$\Delta f, \Delta f_{\mathrm{D}}$	(1) rf received signal and Doppler signal bandwidths; (2) expected errors in the estimation of those frequencies; (3) Δf also denotes the frequency interval taken in the DFT calculation

Acknowledgments

We are indebted to Professor Antoni Ras, of the Department of Applied Mathematics and Telematica at the Universitat Politècnica de Catalunya, for his invaluable assistance in the derivation of several of the mathematical expressions employed throughout this work.

References

1. D. Liepsch, A. Poll, and G. Pflugbeil, ''In vitro laser anemometry blood flow systems,'' in *Fifth International Conf. on Laser Anemometry: Advances and Applications, Proc. SPIE* **2052**, 163–178 (1993).

2. C. Bertrand and P. Chappet, ''Investigation of the aerodynamic field around a TGV power car by trainborne laser Doppler velocimeter,'' *GEC Alsthom Tech. Rev.*, No. 16, pp. 17–24 (1995).
3. M. W. Nielsen, B. Osmondson, and D. Niccum, ''Accurate, noncontact technique for measuring length and speed of wire and cable,'' in *Proc. Annual Convention of the Wire Association International*, *Proc. Annu. Conv. Wire Assoc. Int.*, pp. 275–281 (1997).
4. M. K. Lyon and L. G. Leal, ''Experimental study of concentrated suspensions in two-dimensional channel flow. Part 1. Monodispersive systems,'' *J. Fluid Mech.* **363**, 22–26 (1998).
5. J. Rheims, T. Wried, and K. Bauckhage, ''Sizing of inhomogeneous particles by a differential laser Doppler anemometer,'' *Meas. Sci. Technol.* **10**(2), 68–75 (1999).
6. R. Scharf, ''A two-component He-Ne laser-Doppler anemometer for detection of turbulent Reynolds stresses and its application to water and drag-reducing polymer solutions,'' *Meas. Sci. Technol.* **5**(12), 1546–1550 (1994).
7. D. Trimis and A. Melling, ''Improved laser Doppler anemometry techniques for two-point turbulent flow correlations,'' *Meas. Sci. Technol.* **6**(6), 663–673 (1995).
8. H. R. E. van Maanen and A. Oldenziel, ''Estimation of turbulence power spectra from randomly sampled data by curve-fit to the autocorrelation function applied to LDA,'' *Meas. Sci. Technol.* **9**(3), 458–467 (1998).
9. L. H. Benedict and R. D. Gould, ''Enhanced power spectrum estimates using Kalman reconstruction,'' *J. Fluids Eng.* **120**(2), 253–256 (1998).
10. X. Zhang, ''Turbulence measurements of a longitudinal vortex generated by an inclined jet in a turbulent boundary layer,'' *J. Fluids Eng.* **120**(4), 765–771 (1998).
11. L. E. Drain, *The Laser Doppler Technique*, Addison-Wesley (1975).
12. Dantec Measurement Technology A/S, *Principles of Laser Doppler Anemometry*, www.dantecmt.com/lda/Princip (1997).
13. Y. Ikeda and T. Nakajima, ''Burst digital correlator as laser-Doppler velocimetry signal processor,'' *Appl. Opt.* **35**(18), 3243–3249 (1996).
14. P. M. Howard and R. V. Edwards, ''Implementation of a likelihood ratio test for laser Doppler velocimeter burst detection,'' *Appl. Opt.* **36**(30), 7629–7638 (1997).
15. A. V. Oppenheim and R. W. Schafer, *Discrete-Time Signal Processing*, Prentice-Hall (1989).
16. D. C. Montgomery, G. C. Runger, and N. F. Hubele, *Engineering Statistics*, Wiley (1998).
17. A. Papoulis, *Probability, Random Variables and Stochastic Processes*, 3rd ed., McGraw-Hill (1991).
18. D. C. Rife and R. R. Boorstyn, ''Single-tone parameter estimation from discrete-time observations,'' *IEEE Trans. Inf. Theory* **IT-20**(3), 591–598 (1975).
19. H. H. Qiu, M. Sommerfeld, and F. Durst, ''Two novel Doppler signal detection methods for laser Doppler and phase Doppler anemometry,'' *Meas. Sci. Technol.* **5**(7), 769–778 (1994).

Federico Dios received his Engineer degree in 1986 and his Dr Eng degree in 1992 from the Telecommunication Engineering School of Barcelona. He is titular professor at the Universitat Politècnica de Catalunya. His current research interests are laser Doppler anemometry, optical range-finding, and obstacle detection.

Adolfo Comerón received a telecommunication engineer degree from the Telecommunication Engineering School of Barcelona in 1976, and DEA and DrEng degrees from the Paris-XI University, Orsay, in 1977 and 1980, respectively. He is currently professor at the Technical University of Catalonia, Barcelona, Spain. His research activities have included the study of nonlinear devices at IR wavelengths and the development of microwave and millimeter-wave receivers for satellite communication systems. They currently focus on free-space optical communications and remote detection and sensing at optical wavelengths.

David García-Vizcaíno received a degree in telecommunications in 1993 and the Telecommunication Engineering degree in 1998, both from the Technical University of Catalonia (UPC). Since 1996 he has been an Associate Professor with the Department of Signal Theory and Communications (UPC). His research interests include low-power coherent laser radar and laser Doppler anemometry systems.